

# Spatial-Temporal Synergic Residual Learning for Video Person Re-Identification

Xinxing Su<sup>1\*</sup> Yingtian Zou<sup>1\*</sup> Yu Cheng<sup>2</sup> Shuangjie Xu<sup>1</sup>  
Mo Yu<sup>3</sup> Pan Zhou<sup>1</sup>

<sup>1</sup> Huazhong University of Science and Technology, <sup>2</sup>Microsoft AI & Research

<sup>3</sup>IBM Research AI

(\* denotes equal contribution)

**Abstract.** We tackle the problem of person re-identification in video setting in this paper, which has been viewed as a crucial task in many applications. Meanwhile, it is very challenging since the task requires learning effective representations from video sequences with heterogeneous spatial-temporal information. We present a novel method - Spatial-Temporal Synergic Residual Network (STSRN) for this problem. STSRN contains a spatial residual extractor, a temporal residual processor and a spatial-temporal smooth module. The smoother can alleviate sample noises along the spatial-temporal dimensions thus enable STSRN extracts more robust spatial-temporal features of consecutive frames. Extensive experiments are conducted on several challenging datasets including iLIDS-VID, PRID2011 and MARS. The results demonstrate that the proposed method achieves consistently superior performance over most of state-of-the-art methods.

**Keywords:** Video Person Re-ID, Residual Learning, Spatial-Temporal Information

## 1 Introduction

Person Re-identification (ReID) is the problem of associating different tracklets of a person across non-overlapping cameras. It has become increasingly popular for its crucial applications in visual surveillance and human computer interaction. Benefited from tremendous success of deep learning, the computer vision field has witnessed the prominent progresses in image-based person re-ID [1,2,3], which only utilizes the spatial information. However, single-shot appearance features of people are intrinsically limited to the inherent visual ambiguity. More recently, many attentions have been shifted to the video re-ID since its natural setting and some benefits with sequential information.

Video re-ID faces several significant challenges, like cluttered backgrounds, out-of-focus targets, misalignments and large appearance changes as a person moves between cameras. In a meanwhile, how to extract more comprehensive representations, particularly incorporate spatial and temporal information available in videos, is still under-studied. To overcome the these issues, recent video-based

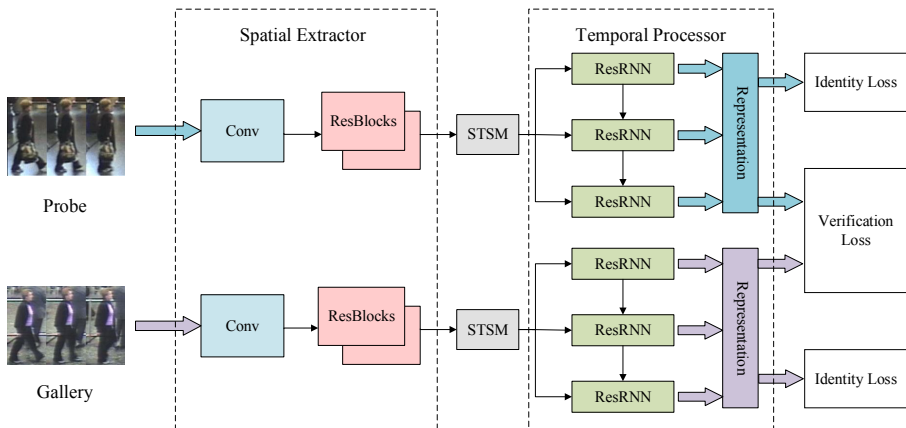


**Fig. 1.** Overview of Spatial-Temporal Synergic Residual learning Network (STSRN). The framework extracts the generic and specific spatial-temporal features of consecutive frames with the help of synergic residual learning between spatial residual blocks, spatial-temporal smooth module (STSM) and residual RNN (ResRNN)

methods have tended to utilize RNNs [4] (or CNN-RNNs) to take consecutive frames as inputs, and adaptively incorporate temporal information [5,6,7,8,9,10,11]. For instance, [11,8] focus on considering the mutual influence between video sequences. On the other hand, another frequently used strategy is the multi-shot matching [12,13,14,15], where they only utilize convolution-based representations. Pooling operation in these methods aggregates frame-level features into a global vector, which has demonstrated its simplicity but effectiveness. However, the residual learning in CNN or RNN is rarely studied in the literature related to person ReID.

To tackle with aforementioned issues, we propose Spatial-Temporal Synergic Residual Network (STSRN), a novel method aiming at solving the coherent representation learning bottlenecks on existing spatial-temporal models. This is achieved by exploring three different modules: a spatial residual extractor, a temporal residual processor and a spatial-temporal smoother. Particularly, the spatial residual extractor can extract discriminative frame-level spatial features while temporal processor could further improve the ability of modelling long-range dependencies and eliminate redundancy in videos with the help of residual learning. The spatial-temporal smoother makes a gentle transition between spatial domain and temporal domain.

Moreover, our proposed model provides an end-to-end and parameter-efficient solution. Instead of extracting frame-level representations by using GoogLeNet [16] such as in [15] and [10], or time-consuming in inference stage [11,8], we employ a much smaller architecture in that STSRN could be more likely to apply to real-time video surveillance system.

In summary, our main contributions are in three-folds:

- We propose the Spatial-Temporal Smooth Module (STSM) for straining to eliminate the noise interference in embeddings when transformed from spatial domain into temporal domain. STSM demonstrates its effectiveness theoretically and experimentally in spatial-temporal synergic residual learning.
- We devise a new spatial-temporal network which has a better representation than other CNN-RNNs. Compared with most previous approaches, STSRN is very parameter saving and efficient for both training and prediction.
- We evaluate STSRN on three popular video benchmark datasets, iLIDS-VID, PRID2011 and MARS. The experimental results show that our model beat most of state-of-art approaches with much fewer parameters. To prove the validity of model, we also perform cross-dataset testing on PRID2011.

## 2 Related Work

Person re-identification has been a hot topic. Especially in recent years, video-based person re-ID task has drawn increasing attention due to its practicability in surveillance. In video-based re-ID, each tracklet contains a number of frames rather a single image. Comparing with single shot person re-ID, video-based fashion utilizes more potential information thus has a better prospect. Previous work on video person re-ID can be roughly categorized into two classes: hand-crafted feature based methods [17,18,19,20,9,21,22] and deep learning based methods [3,8,23,24,5,7,15,10,13].

Classical separate solutions target at feature extraction [17,18,19] and distance metric learning [9,21]. For feature extraction, Wang *et al.* [19] represent video fragments by the HOG3D features and the average color histograms, where they screen these discriminative fragments from noisy sequences by estimating the flow energy profile (FEP). By distance metric learning, Liu *et al.* [20] consider spatial alignment and temporal alignment to treat the appearance of different body parts independently. They then represent feature using fisher vector.

Deep methods can be further subdivided into two aspects: (1) The methods focusing on spatial image-level representations [15,13], which generally build tremendous and complex networks. For example, Liu *et al.* [15] directly learn to automatically score the image data according to its quality. Zheng *et al.* [13] tries to train a classification network [25] where each single image is represented by a feature vector. It is inevitable to establish a deeper and complicated hierarchy in their models. (2) The ones paying more attention to temporal sequence-level representations, most of which adopt CNN-RNNs [5,13,10,7,6,8,11]. Pooling based strategies in these models aggregate the features of tracklet which have better scalability in the sequence level. Dai *et al.* [10] employ double GoogLeNets [16] to extract general features and aligned features, which are processed by double Bi-LSTMs [26] separately. It also propose a spatial-temporal transformer network (ST<sup>2</sup>N) to fuse different level features from the a GoogLeNet. Xu *et al.* [8] propose an jointly spatial-temporal attention matrix to maximum the relativity of different scene feature. Chung *et al.* [7] process spatial information and motion information separately by SpatialNet and TemporalNet.

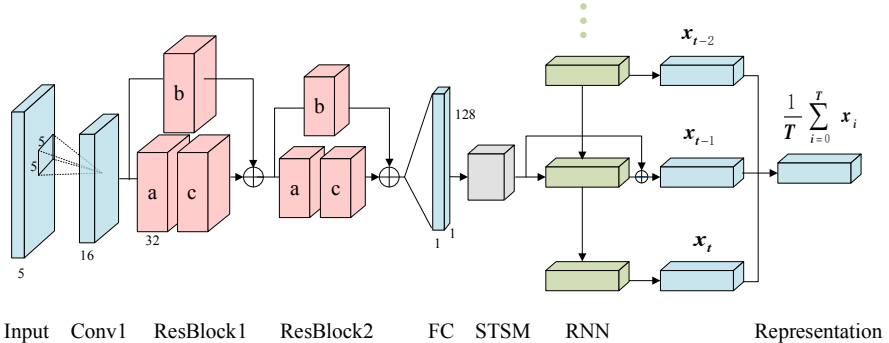


**Fig. 2.** Details of the network structure. Kernel size, stride and padding of cube “a, b” are 5, 4 and 1, respectively. Kernel size, stride and padding of cube “c” are 3, 1 and 1, respectively. “ $\oplus$ ” is element-wise addition.

As predicted in the Zheng *et al.*'s survey [23], recent multi-shot based re-ID methods reporting competitive accuracy mainly adopt the discriminative combination of appearance and spatial-temporal models or directly fine-tuned an identification model pretrained in ImageNet [27]. With the increase in capacity of spatial representation, they intensify the risk of over-fitting and time complexity. Meanwhile, deep residual learning has achieved tremendous success in various visual tasks [24,28,29,30]. In Feichtenhofer *et al.*' work [30], it builds on injecting residual connections from appearance into motion pathway in a two-stream convolutional networks. Utilizing additive merging of signals can ease the training of network which has an advantage of informative tasks like video analysis. Instead of fusing different level features for learning aligned features [10], we devise a unidirectional spatial residual extractor to perform progressively fusion layer by layer. For the purpose of a better representation with parameter saving fashion than other CNN-RNNs, we propose a spatial-temporal synergic residual network which can reduce the both information redundancy and noisy interference.

### 3 The Proposed Model Architecture

#### 3.1 Overview

Our proposed framework, STSRN, belongs to the spatial-temporal models. As shown in Figure 1, our STSRN is trained as a Siamese network architecture [17] by passing a pair of image sequences, each of which is a slice of the tracklet. After the fully-connected layer, it produces an embedding for every image and then be smoothed by the STSM. For these embeddings, the temporal residual processor would generate the frame-level features, which will then be aggregated

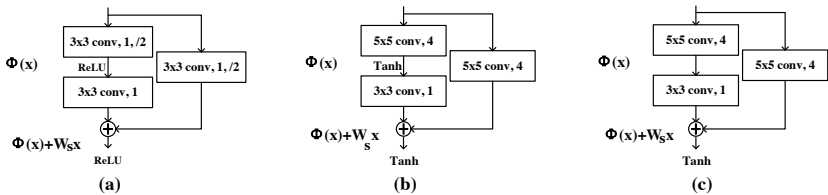


**Fig. 3.** Comparisons on different structures of residual blocks. The digits in rectangle indicate kernel size, layer type, padding and stride (if exists), respectively. (a) Residual connection in ResNet [24], (b) Variant of (a) with larger kernel size and padding, and Tanh activation, (c) The same architecture as (b) without in-block activation

into the sequence-level representation. Overall, the network outputs two global vectors for computing the Euclidean distance between them and predicting the probability distribution over training identities.

There are two crucial parts and an interlayer between them. The first one lies in residual blocks, which could learn more discriminative features than the plain counterpart. Compared with the standard forms of the ResNet [24], our residual blocks are more suitable for re-ID tasks on hand, as will be explained below. Introducing residual learning into RNN brings further performance gains and robustness. Meanwhile, the smoother guides the temporal processor to focus on the most relevant frames for matching with a novel gating mechanism.

### 3.2 Spatial Residual Extractor

Recently, the state-of-the-art multi-shot re-ID methods tend to adopt complex hierarchies such as Two Stream Siamese Networks [7], QAN [15] and TRL [10]. With more learnable parameters, these methods have potential superiority in terms of model capacity but leads to higher risk of over-fitting and time complexity. This section proposes a new spatial feature extractor, which both simplifies the model topology and improves the discriminability of the representation for video-based re-ID task.

From Figure 2, we can see that the spatial extractor can be divided into three submodules: one for convolutional and the others for residual submodules. Specifically, each submodule is composed of filter banks, hyperbolic-tangent (Tanh) activation-function and max-pooling. The input to the network consists of both optical flow channels and colour channels. Given the input sequences  $S = \{I^\tau \in \mathbb{R}^{w \times h \times c} | \tau = 1, \dots, T\}$ , the first submodule outputs feature maps  $C'(S)$ , where  $T$  is the sampling length of sequence and  $C'(S) = \text{Tanh}(\text{Maxpool}(\text{Conv}(S)))$ .

As shown in Figure 3, instead of applying the standard form from ResNet [24], we adopt  $c$  as our residual module for three purposes. Firstly, we use the Tanh rather than Rectified Linear Unit (ReLU) in residual blocks to keep the data distribution compatible with subsequent recurrent layer. Secondly, removing the activation layer inside the residual block alleviates the gradient vanishing problem caused by Tanh. Last but not the least, this layout has larger kernel size

and padding, which are more applicable on low-resolution video ReID task. Compared to [5], the introduction of residual blocks offers more paths for information flowing from early layer to later layer. Formally, the feature set of the residual submodule can be formulated as follow:

$$f_{res}^k(x) = \Phi(x) + W_s x \quad (1)$$

where  $x$  and  $k$  represents the input to to the block, and the index of blocks, respectively. Next, the embeddings  $f_s(S) = \{f_s(I^\tau) \in \mathbb{R}^N, \tau = 1, \dots, T\}$  are mapped by the fully-connected layer, where  $N$  is the dimensionality of embeddings and  $f_s$  a series of non-linear mapping from the raw pixels to a new embedding space.

### 3.3 Spatial-Temporal Smooth Module

Because of the challenges such as occlusions and background clutter in video person re-ID, it is necessary to simultaneously make full use of space and temporal information [23]. For this, a Spatial-Temporal Smooth Module (STSM) is introduced to discard noisy motion occurring over a short period through selecting most salient spatial features temporally.

Following Section 3.2, we obtain spatial embedding set  $f_s(S)$ , whose adjoining embeddings are then fused by learnable parameters  $\theta$  and  $\omega$ . More specifically, the sum of each element of  $\theta$  and  $\omega$  is subject to one. Therefore, the smoother aggregates  $f_s(I^{\tau-1})$  and  $f_s(I^\tau)$  temporally as follow:

$$f_{s \rightarrow t}^\tau = \theta \odot f_s(I^\tau) + \omega \odot f_s(I^{\tau-1}) \quad (2)$$

$$= f_s^\tau + \omega \odot (f_s^{\tau-1} - f_s^\tau) \quad (3)$$

where  $\omega \in \mathbb{R}^N$  and  $f_{s \rightarrow t}^1 = f_s^1$ .  $\omega$  serve as gate mechanism: when some frame is interference, the mechanism would balance the ratio of information flow, thus guiding the recurrent layer to focus on more discriminate features.

### 3.4 Temporal Residual Processor

Inspired by the residual spatial connections, we also consider to employ residual learning temporally to further help the re-ID task. As shown in Figure 2, we introduce a shortcut connection from the output of STSM to the output of the RNN. On one hand, RNN allows informative data to propagate from the first time step to the last one and accumulates discriminative information along the temporal dimension. On the other hands, through alternative information of current frame, the residual connection can prevent redundant information from worsening the temporal accumulation, which makes it more robust to noisy motion. Furthermore, this novel fashion is parameter-free.

For simplicity, we reformulate the embeddings produced by fully-connected layer as  $[x^1, x^2, \dots, x^T]$ , and then obtain smoothed embedding matrix  $M$  transited by STSM:

$$M = [\hat{x}^1, \hat{x}^2, \dots, \hat{x}^T], \hat{x}^\tau = f_{s \rightarrow t}^\tau \quad (4)$$

Thus, we can incorporate recurrent connections between the STSM and temporal-pooling layer as follows:

$$\hat{o}^\tau = U\hat{x}^\tau + Vr^{\tau-1} \quad (5)$$

$$o^\tau = \frac{\hat{o}^\tau + \hat{x}^\tau}{2}, r^\tau = \text{Tanh}(o^\tau) \quad (6)$$

where  $r^\tau \in \mathbb{R}^L$  is the hidden state at time  $\tau - 1$ , and  $o^\tau \in \mathbb{R}^L$  is the output at time  $\tau$ ,  $U \in \mathbb{R}^{N \times L}$  and  $V \in \mathbb{R}^{L \times L}$  are the projection weights for the observation  $\hat{x}^\tau$  and previous hidden state, respectively. Next, all outputs of the residual RNN are performed mean-pooling over the temporal dimension to produce a global feature vector  $v_g$  characterizing the whole input:

$$v_g = \frac{1}{T} \sum_{\tau} o^\tau \quad (7)$$

Our residual connections in RNN provide alternative signals, which make the training of RNN an easier problem, i.e., the features are smoothly transferred across video sequence. Besides, it further reduces the information redundancy beyond the benefits of STSM.

### 3.5 Training Objective

Given a pair of input sequences  $(S^m, S^n)$  of persons  $m$  and  $n$ , our STSRN produces two global spatial-temporal vectors  $(v_g^m, v_g^n)$ . Note that  $S^m$  and  $S^n$  could be of different lengths. We define our training objective on the joint identification and verification loss from [31]. The verification cost, i.e. siamese cost, tries to minimize the distance between  $v_g^m$  and  $v_g^n$  when they belongs to the same identity and maximize the distance otherwise:

$$\mathcal{L}_{veri}(v_g^m, v_g^n) = \begin{cases} \|v_g^m - v_g^n\|_2^2, & p = g \\ \max(0, m - \|v_g^m - v_g^n\|_2), & p \neq g \end{cases} \quad (8)$$

where  $m$  is the margin. Besides, we apply the cross-entropy loss to obtain the identity cost on persons  $p$  and  $g$  as  $\mathcal{L}_{iden}(v_p)$  and  $\mathcal{L}_{iden}(v_g)$ . The total training objective is the sum of these cost.

## 4 Experiments

This section empirically compares our proposed framework with previous state-of-the-art methods for video-based person re-identification on three popular benchmarks: iLIDS-VID [19], PRID2011 [32] and MARS [13]. We also conduct analysis to better understand the effects of several crucial components and parameter settings.

## 4.1 Datasets

**iLIDS-VID dataset.** The iLIDS-VID dataset [19] consists of 300 distinct pedestrians with one pair of sequences from two non-overlapping camera perspectives for each person. It was captured at a crowded airport arrival hall with significant background clutter, extremely heavy occlusion and viewpoint/illumination variations across camera views, which makes it one of the most challenging datasets used for multi-shot person re-ID task. The length of each image sequence varies from 23 to 192, with an average number of 73 images.

**PRID2011 dataset.** Although also featuring multiple person trajectories from two different, static surveillance cameras similar to the former, PRID2011 [32] has different number of identities for Camera A and Camera B, respectively. Only the first 200 persons appear in both views, which results in 400 image sequences totally, and it was captured in uncrowded outdoor scenes with relatively simple backgrounds and rare occlusions. The length of consecutive frames in single camera view for each person ranges 5 to 675, with an average number of 100.

**MARS dataset.** The Motion Analysis and Re-identification Set (MARS) [13] is a large-scale video dataset which contains 1,261 different identities in over 20,000 tracklets. These tracklets are automatically generated by the pedestrian detector DPM and tracker GMMCP making it more realistic and challenging than datasets above. Most IDs are captured by 2-4 cameras and camera-2 produces the most tracklets. Most tracklets contain 25-50 frames, and there are 13.2 tracklets on average for each identity.

## 4.2 Implementation Details

For these experiments, we randomly split each dataset into two non-overlapping subsets with same amount of identities for training and testing, respectively. The results are reported using the average *Cumulative Matching Characteristics* (CMC) curves under “10-fold cross validation”. In the testing phase, the probe set and the gallery set contain data from two different cameras for iLIDS-VID and PRID2011; and we only use the first 200 identities appeared in both cameras for PRID2011. As for MARS, we randomly chose 2 cameras of the same person out of the ensemble following [8]. For the fairness comparison, we set the sampling length of each person sequence to 16 and 128 for training and testing, respectively.

Data preprocessing contained several steps [8]: The optical flow channels were calculated between each pair of images horizontally and vertically by Lucas-Kanade algorithm [33] then normalized to fall within the range -1 to 1 while the RGB images were converted to YUV color space. Both the RGB channels and flow channels were normalized to the range of [0,1], after which another normalization operation was applied to have zero mean and unit variance channel by channel to keep the consistency of the influence of each feature on the objective function.

**Table 1.** Comparisons of our network with other state-of-the-art methods on iLIDS-VID and PRID2011 in terms of CMC rank-1, rank-5, rank-10 and rank-20 (%).

Model	iLIDS-VID				PRID2011			
	R1	R5	R10	R20	R1	R5	R10	R20
VR[19]	34.5	56.7	67.5	77.5	37.6	63.9	75.3	89.4
SI <sup>2</sup> D[9]	48.7	81.1	89.2	97.3	76.7	95.6	96.7	98.9
TDL[21]	56.3	87.6	95.6	98.2	56.7	80.0	87.6	93.5
RFA[35]	49.3	76.8	85.3	90.0	58.2	85.8	93.4	97.9
CNN-RNN[5]	58.0	84.0	91.0	96.0	70.0	90.0	95.0	97.0
RCN+KISSME[36]	46.1	76.8	89.7	95.6	69.0	88.4	93.2	96.4
TSSCNN[7]	60.0	86.0	93.0	97.0	78.0	94.0	97.0	99.0
ASTPN[8]	62.0	86.0	94.0	98.0	77.0	90.0	95.0	99.0
CNN+XQDA[13]	53.0	81.4	-	95.1	77.3	93.5	95.7	99.3
SRM+TAM[11]	55.2	86.5	-	97.0	79.4	94.4	-	99.3
QAN*[15]	68.0	86.8	95.4	97.4	<b>90.3</b>	<b>98.2</b>	<b>99.3</b>	<b>100</b>
TRL[10]	57.7	81.7	-	94.1	87.8	97.4	-	99.3
STSRN	<b>70.0</b>	<b>89.3</b>	<b>95.7</b>	<b>98.7</b>	88.0	97.0	99.0	99.0

- “\*” indicates that the number of frames in tracklet is larger than 21 are used in PRID2011, which is different from common settings.

The training sequences were augmented in the form of randomly cropping and mirroring, which was applied to all frames of a given sequence to improve the ability of generalization. We also adopted the same augmentation step in test phase. Following [8], image sequences from different cameras of same pedestrian were considered as positive pairs while those of different pedestrians negative pairs. The positive and negative pairs were alternatively fed into the network.

The initialization of weight parameters for convolutional layers and fully-connected layers was done by Xavier method [34]. The hyper-parameters were set based on [5] except that init learning rate was set to  $2 \times 10^{-3}$ . With the stochastic gradient descent (SGD) algorithm, the proposed model was trained on NVIDIA GTX-1080Ti GPUs.

### 4.3 Comparison with the State-of-the-Art

To further evaluate the performance of our model, we compared the proposed architecture with the state-of-the-art methods on iLIDS-VID, PRID2011 and MARS datasets.

**Results on iLIDS-VID and PRID2011.** Table 1 shows results on iLIDS-VID and PRID2011 datasets. The upper part lists the state-of-the-art methods with hand-crafted features while the middle part displays recent video-based methods under the scope of deep learning. With the help of the novel spatial-

**Table 2.** Comparisons on MARS in terms of CMC matching rate (%).

Model	MARS			
	R1	R5	R10	R20
CNN-RNN[5]	40.0	60.0	70.0	77.0
ASTPN[8]	44.0	70.0	74.0	81.0
STSRN	<b>76.7</b>	<b>93.8</b>	<b>96.8</b>	<b>98.1</b>

**Table 3.** Comparisons on the number of parameters of models

Models	CNN-RNN[5]	TSSCNN[7]	QAN[15]	TRL[10]	Ours
Parameters	430k	860k	6.7M	≈30M	590k

temporal residual learning framework, our STSRN, listed at the bottom, outperforms all previous methods on the challenging iLIDS-VID task, and most of them on PRID2011 in terms of the CMC results. Note that our network surpasses the state-of-the-art comprehensively and transcends TRL [10] by 12.3%, 8.4% and 4.6% on iLIDS-VID in terms of rank-1, rank-5 and rank-20 matching rate, which strongly demonstrates the effectiveness of our synergic residual learning across spatial domain and time domain. Compared to the QAN [15], our network achieves 70.0% matching rate at rank-1, exceeding it by 2% with much lower complexity both in network architecture and query time. Besides, our STSRN also remains substantially ahead in PRID2011 where our model set the new state-of-the-art under the common settings.

**Results on MARS.** As shown in Table 2, our STSRN outperforms ASTPN [8] and CNN-RNN [5] by a large margin on MARS. More explicitly, our STSRN surpasses ASTPN and CNN-RNN by 32.7% and 36.7% at CMC rank-1 matching rate, respectively, which demonstrates superior performance of our STSRN on challenging video ReID dataset again.

**Complexity** As far as computing saving is concerned, our model is superior to competitor methods about the number of parameters; for a better illustration of this, Table 3 directly quantifies the previous state-of-the-arts and ours. It could be easily concluded that STSRN has a comprehensive advantage over others, and its parameters are only one tenth of GoogLeNet [16]. Compared to previous research that usually strike a balance between the model complexity and characterization capability, our model is both light-weighted and high-performing network, mainly by benefiting from the synergic residual learning.

**Efficiency.** Most model with attention mechanism [11,8] suffer from grossly inefficient computation because of the mutual influence between the query and the gallery. However, our system employs pre-computing tactic, i.e., features

**Table 4.** Cross-Dataset Testing on PRID2011 in terms of CMC rank1/5/10/20

Method	R1	R5	R10	R20
CNN-RNN [5]	28.0	57.0	69.0	81.0
ASTPN [8]	30.0	58.0	71.0	85.0
TRL [10]	29.5	59.4	-	82.2
STSRL	32.0	58.0	71.0	90.0

of identities are extracted as the memory. When a query comes, the system merely rank the distance between the memory and current query. Suppose we have  $X$  examples to query and  $Y$  examples in the gallery. The attention-based approaches need to extract features for  $XY$  times while we only need  $X + Y$  times.

#### 4.4 Cross-Dataset Generalization

Due to the variety of geometric and environmental conditions, models trained on one dataset maybe exhibit poor performance on another, due to the over-fitting trap. To better evaluate the generality of our model, we conducted cross-dataset experiments which were trained on iLIDS-VID and tested on PRID2011, showing the results in Table 4. We achieve 32.0%, 58.0%, 71.0% and 90.0% of the CMC scores at rank-1, 5, 10 and 20, exceeding all baselines except for being slightly inferior to TRL method at rank-5, which proves certain generality of our model.

#### 4.5 Effectiveness of Spatial Residual Blocks

As shown in Figure 2, our spatial submodule contains double residual blocks. Inspired by the strong evidence shown in [24], we also expected that the residual learning principle could be generalized to our re-ID task. We performed experiments mainly related to the number and form of spatial residual blocks. The description of experimental models and their CMC curves from rank-1 to rank-20 are illustrated in Table 5 and Figure 4, respectively.

From the CMC curves in Figure 4, we have three important observations. First, the introduction of adequate residual blocks in the form of Figure 3c can significantly boost the CMC accuracy from rank-1 to rank-20. Specifically, both *DoubleResBlocks* and *SingleResBlock* surpass *BaseModel* without any residual connections by a large margin for iLIDS-VID. Besides, the rank-1 matching rate of *DoubleResBlocks* and *SingleResBlock* for PRID2011 outperforms that of *BaseModel* by 11.0% and 8.0%, respectively, and even for the more challenging iLIDS-VID, the rank-1 accuracy is improved by about 6.7% when *BaseModel* changes to *DoubleResBlocks*. Second, it is not better to simply add more residual blocks. The CMC curve of *TripleResBlocks* performs worse than *DoubleResBlocks* on two datasets in highest ranks. Third, the rank-1 accuracies fall down to just 56.3% and 71.0% for iLIDS-VID and PRID2011, respectively when the architecture

**Table 5.** Comparable models for exploring how to make full use of spatial residual connections. All models are followed by a fully-connected layer and the vanilla recurrent neural network. The “Conv”, “Res” and “Res\*” are the convolutional layer, the residual block of Figure 3c and Figure 3a, respectively, which are all followed by a Tanh layer. The kernel size, padding and stride of “Conv”s are set to 5, 4 and 1, respectively. The “Max” is the max pooling layer with window size 2 and stride 2

Model	Layer	Max	Layer	Max	Layer	Max	Layer	Max
BaseModel	Conv	+	Conv	+	Conv	+	-	-
SingleResBlock	Conv	+	Conv	+	Res	+	-	-
DoubleResBlocks	Conv	+	Res	+	Res	+	-	-
TripleResBlocks	Conv	+	Res	-	Res	+	Res	+
DoubleResBlocks*	Conv	+	Res*	+	Res*	+	-	-

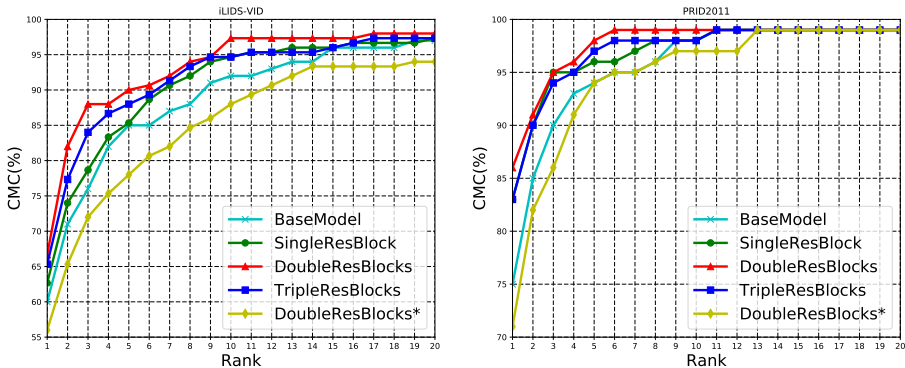


**Fig. 4.** CMC curves of different numbers and different kinds of spatial residual blocks on (a) iLIDS-VID and (b) PRID2011 datasets

moves from Figure 3c to Figure 3a, which demonstrates that larger receptive field and the max pooling are more suitable for our tasks.

In addition, when we replaced the residual blocks of *DoubleResBlocks* with Figure 3b, the CMC scores at rank-1 was stuck at 63.3% for iLIDS-VID, which is inferior to that of *TripleResBlocks*. It reflects the gradient vanishing problem caused by *Tanh*.

#### 4.6 Evaluation on Temporal Residual Learning

Due to significant viewpoint/illumination variations as well as background clutter and occlusions, a good video-based re-ID method should grab these diversities selectively, especially the temporal cues. To illustrate how our temporal residual learning works, we display the rank-1 matching rate curves with the progress of training in Figure 5, and record CMC rank-1, rank-5, rank-20 scores at Table 6.

**Table 6.** CMC scores in terms of rank-1, rank-5, rank-20 for *BaseModel* and *DoubleResBlocks* with/without residual RNN or STSM on iLIDS-VID and PRID2011 datasets. The “TemRes” and “STSM” mean temporal residual learning and the Spatial-Temporal Smooth Module, respectively

Dataset	iLIDS-VID			PRID2011		
Rank	1	5	20	1	5	20
BaseModel	60.3	87.7	96.7	75.0	95.0	98.0
DoubleRes	66.7	89.3	97.3	86.0	96.0	99.0
Base+TemRes	61.3	88.3	97.7	78.0	93.0	99.0
Double+TemRes	68.7	90.0	98.3	87.0	97.0	99.0
Base+TemRes+STSM	63.7	87.3	98.7	80.0	96.0	99.0
Double+TemRes+STSM	70.0	89.3	98.7	88.0	97.0	99.0

From Figure 5, it can be easily observed that the residual learning in RNN brings considerable performance gains along with the powerful ability of noise resistance for both *BaseModel* and *DoubleResBlocks* during the training phase. Specifically, *BaseModel* only reaches an accuracy of 28.3% in the 100<sup>th</sup> training epoch while *BaseModel+TemRes* greatly improves on that, achieving an accuracy of 46.7%. More clearly, the *DoubleResBlocks+TemRes* substantially shows smaller jitter and possesses slightly higher accuracy than its counterpart overall.

From Table 6, we can see that the temporal residual learning improves CMC scores for *BaseModel* on both datasets. With the help of the residual RNN, there are 1.0% and 3.0% lift at rank-1 score on iLIDS-VIDS and PRID2011, respectively for *BaseModel* while 2.0% and 1.0% for *DoubleResBlocks*.

In a word, our temporal residual processor actually helps to prevent redundant information from worsening discriminative feature extraction. In other words, the models equipped with residual connections temporally grab diversities across video sequence selectively, making it more robust to noisy features.

#### 4.7 Discussion about STSM

As illustrated in Section 3.3, we devise the STSM to smooth noisy motion in adjoining frames. Here we compare models whether assembled with STSM or not at Table 6. More detailed tendency of the CMC curves are shown in Figure 5. As we expect, models with STSM outperform ones without STSM. For example, *BaseModel+TemRes+STSM* is about 2% higher than *BaseModel+TemRes* on both datasets while there are 1.3%, 1.0% improvements for *DoubleRes* in terms of rank-1 matching rate on iLIDS-VID, PRID2011, respectively. These evidence experimentally illustrate that STSM can effectively enhance spatial-temporal synergic residual learning.

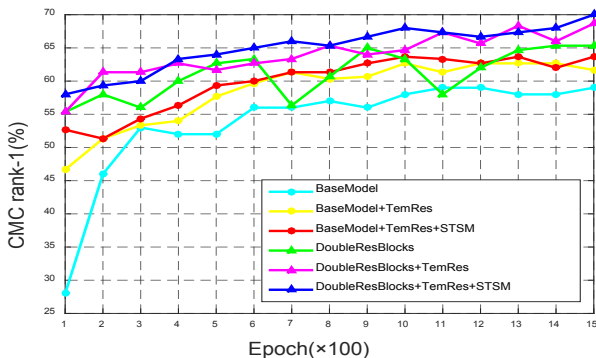


**Fig. 5.** CMC scores at rank-1 with the progress of training for *BaseModel* and *DoubleResBlocks* models with/without residual RNN or STSM on iLIDS-VID. The “TemRes” and “STSM” means temporal residual learning and the Spatial-Temporal Smooth Module, respectively

## 5 Conclusions

In this paper we develop a succinct but powerful framework, Spatial-Temporal Synergic Residual Network (STSRN), for video-based person re-identification. Our spatial residual blocks effectively extract spatial features for single image and the recurrent residual learning module provides alternative signals. Besides, the parameter-efficient spatial-temporal smooth module (STSM) can further improve the robustness of the model. Both extensive experiments results and detailed analyses on MARS, iLIDS-VID and PRID2011 datasets strongly demonstrate that STSRN breaks through the bottlenecks in small spatial-temporal networks for person re-id. STSRN would be adapted to person detection and tracking tasks in the future [37].

## References

1. Liao, S., Hu, Y., Zhu, X., Li, S.Z.: Person re-identification by local maximal occurrence representation and metric learning. In: CVPR. (2015) 2197–2206
2. Zhao, R., Ouyang, W., Wang, X.: Unsupervised salience learning for person re-identification. In: CVPR. (2013) 3586–3593
3. Ahmed, E., Jones, M., Marks, T.K.: An improved deep learning architecture for person re-identification. In: CVPR. (2015) 3908–3916
4. Rumelhart, D.E., Hinton, G.E., Williams, R.J.: Learning representations by back-propagating errors. *nature* **323**(6088) (1986) 533
5. McLaughlin, N., del Rincon, J.M., Miller, P.: Recurrent convolutional network for video-based person re-identification. In: CVPR. (2016) 1325–1334
6. Yu, Z., Li, T., Yu, N., Gong, X., Chen, K., Pan, Y.: Three-stream convolutional networks for video-based person re-identification. arXiv preprint arXiv:1712.01652 (2017)

7. Chung, D., Tahboub, K., Delp, E.J.: A two stream siamese convolutional neural network for person re-identification. In: CVPR. (2017) 1983–1991
8. Xu, S., Cheng, Y., Gu, K., Yang, Y., Chang, S., Zhou, P.: Jointly attentive spatial-temporal pooling networks for video-based person re-identification. arXiv preprint arXiv:1708.02286 (2017)
9. Zhu, X., Jing, X.Y., Wu, F., Feng, H.: Video-based person re-identification by simultaneously learning intra-video and inter-video distance metrics. In: IJCAI. (2016) 3552–3559
10. Dai, J., Zhang, P., Lu, H., Wang, H.: Video person re-identification by temporal residual learning. arXiv preprint arXiv:1802.07918 (2018)
11. Zhou, Z., Huang, Y., Wang, W., Wang, L., Tan, T.: See the forest for the trees: Joint spatial and temporal recurrent neural networks for video-based person re-identification. In: CVPR, pages=6776–6785, year=2017,
12. Bazzani, L., Cristani, M., Perina, A., Farenzena, M., Murino, V.: Multiple-shot person re-identification by hpe signature. In: Pattern Recognition (ICPR). (2010) 1413–1416
13. Zheng, L., Bie, Z., Sun, Y., Wang, J., Su, C., Wang, S., Tian, Q.: Mars: A video benchmark for large-scale person re-identification. In: ECCV. (2016) 868–884
14. Farenzena, M., Bazzani, L., Perina, A., Murino, V., Cristani, M.: Person re-identification by symmetry-driven accumulation of local features. In: CVPR. (2010) 2360–2367
15. Liu, Y., Yan, J., Ouyang, W.: Quality aware network for set to set recognition. In: CVPR. (2017) 5790–5799
16. Szegedy, C., Liu, W., Jia, Y., Sermanet, P., Reed, S., Anguelov, D., Erhan, D., Vanhoucke, V., Rabinovich, A., et al.: Going deeper with convolutions. In: CVPR. (2015)
17. Hadsell, R., Chopra, S., LeCun, Y.: Dimensionality reduction by learning an invariant mapping. In: CVPR. (2006) 1735–1742
18. Hamdoun, O., Moutarde, F., Stanculescu, B., Steux, B.: Person re-identification in multi-camera system by signature based on interest point descriptors collected on short video sequences. In: Distributed Smart Cameras(ICDSC). (2008) 1–6
19. Wang, T., Gong, S., Zhu, X., Wang, S.: Person re-identification by video ranking. In: ECCV. (2014) 688–703
20. Liu, K., Ma, B., Zhang, W., Huang, R.: A spatio-temporal appearance representation for video-based pedestrian re-identification. In: ICCV. (2015) 3810–3818
21. You, J., Wu, A., Li, X., Zheng, W.S.: Top-push video-based person re-identification. In: CVPR. (2016) 1345–1353
22. Zhang, W., Ma, B., Liu, K., Huang, R.: Video-based pedestrian re-identification by adaptive spatio-temporal appearance model. IEEE transactions on image processing **26**(4) (2017) 2042–2054
23. Zheng, L., Yang, Y., Hauptmann, A.G.: Person re-identification: Past, present and future. arXiv preprint arXiv:1610.02984 (2016)
24. He, K., Zhang, X., Ren, S., Sun, J.: Deep residual learning for image recognition. In: CVPR. (2016) 770–778
25. Jia, Y., Shelhamer, E., Donahue, J., Karayev, S., Long, J., Girshick, R., Guadarrama, S., Darrell, T.: Caffe: Convolutional architecture for fast feature embedding. In: ACM International Conference on Multimedia. (2014) 675–678
26. Schuster, M., Paliwal, K.K.: Bidirectional recurrent neural networks. IEEE Transactions on Signal Processing **45**(11) (1997) 2673–2681
27. Deng, J., Dong, W., Socher, R., Li, L.J., Li, K., Fei-Fei, L.: Imagenet: A large-scale hierarchical image database. In: CVPR. (2009) 248–255

28. Lu, Y., Kumar, A., Zhai, S., Cheng, Y., Javidi, T., Feris, R.S.: Fully-adaptive feature sharing in multi-task networks with applications in person attribute classification. In: 2017 IEEE Conference on Computer Vision and Pattern Recognition, CVPR 2017, Honolulu, HI, USA, July 21-26, 2017. (2017) 1131–1140
29. Ballas, N., Yao, L., Pal, C., Courville, A.: Delving deeper into convolutional networks for learning video representations. arXiv preprint arXiv:1511.06432 (2015)
30. Feichtenhofer, C., Pinz, A., Wildes, R.: Spatiotemporal residual networks for video action recognition. In: NIPS. (2016) 3468–3476
31. Sun, Y., Chen, Y., Wang, X., Tang, X.: Deep learning face representation by joint identification-verification. In: NIPS. (2014) 1988–1996
32. Hirzer, M., Beleznai, C., Roth, P.M., Bischof, H.: Person re-identification by descriptive and discriminative classification. In: Scandinavian conference on Image analysis. (2011) 91–102
33. Lucas, B.D., Kanade, T., et al.: An iterative image registration technique with an application to stereo vision. (1981)
34. Glorot, X., Bengio, Y.: Understanding the difficulty of training deep feedforward neural networks. In: Proceedings of the Thirteenth International Conference on Artificial Intelligence and Statistics(ICAIS). (2010) 249–256
35. Yan, Y., Ni, B., Song, Z., Ma, C., Yan, Y., Yang, X.: Person re-identification via recurrent feature aggregation. In: ECCV, Springer (2016) 701–716
36. Wu, L., Shen, C., Hengel, A.v.d.: Deep recurrent convolutional networks for video-based person re-identification: An end-to-end approach. arXiv preprint arXiv:1606.01609 (2016)
37. Wang, J., Cheng, Y., Feris, R.S.: Walk and learn: Facial attribute representation learning from egocentric video and contextual data. In: CVPR, IEEE Computer Society (2016) 2295–2304